

## **Glial Activation and Glucose Metabolism in a Transgenic Amyloid Mouse Model: A Triple Tracer PET Study**

**Brendel, Matthias<sup>1\*</sup>; Probst, Federico<sup>1\*</sup>; Jaworska, Anna<sup>2</sup>; Overhoff, Felix<sup>1</sup>;  
Korzhova, Viktoria<sup>2</sup>; Albert, Nathalie L.<sup>1</sup>; Beck, Roswitha<sup>1</sup>, Lindner, Simon<sup>1</sup>;  
Gildehaus Franz-Josef<sup>1</sup>; Baumann, Karlheinz<sup>3</sup>; Bartenstein, Peter<sup>1,4</sup>;  
Kleinberger, Gernot<sup>2,4,5</sup>; Haass, Christian<sup>2,4,5</sup>; Herms, Jochen<sup>2,4</sup>; Rominger,  
Axel<sup>1,4</sup>**

<sup>1</sup>Dept. of Nuclear Medicine, Ludwig-Maximilians-University of Munich, Munich, Germany

<sup>2</sup>DZNE - German Center for Neurodegenerative Diseases, Munich, Germany

<sup>3</sup>Roche Pharma Research and Early Development, Neuroscience Discovery, Roche Innovation Center Basel, F. Hoffmann-La Roche Ltd., Basel, Switzerland

<sup>4</sup>SyNergy, Ludwig-Maximilians-University of Munich, Munich, Germany

<sup>5</sup>Biomedical Center (BMC), Ludwig-Maximilians-University of Munich, Munich, Germany

\*both authors contributed equally

**Running title:** Neuroinflammation and amyloidosis in AD mice

### **Corresponding author:**

Prof. Dr. Axel Rominger; Department of Nuclear Medicine; University of Munich; Marchioninistr.15; 81377 Munich, Germany; Phone: +49(0)89440074650; Fax: +49(0)89440077646 ; E-Mail: axel.rominger@med.uni-muenchen.de

### **First author:**

Dr. Matthias Brendel; Department of Nuclear Medicine; University of Munich; Marchioninistr.15; 81377 Munich, Germany; Phone: +49(0)89440074655; Fax: +49(0)89440077646; E-Mail: matthias.brendel@med.uni-muenchen.de

**Word Count:** 4993

**Financial Support:** The study was financially supported by the SyNergy Cluster and by the "Verein zur Förderung von Wissenschaft und Forschung", LMU Munich.

## **ABSTRACT**

Amyloid imaging by small animal PET ( $\mu$ PET) in models of Alzheimer's disease (AD) offers the possibility to track amyloidogenesis and brain energy metabolism. Since microglial activation is thought to contribute to AD pathology, we undertook a triple tracer  $\mu$ PET study to assess microglia activation and glucose metabolism in association with amyloid plaque load in a transgenic AD mouse model.

### **Methods:**

Groups of PS2APP and C57Bl/6 wild-type (WT) mice of various ages were examined by  $\mu$ PET. We acquired 90 min dynamic emission data with  $^{18}\text{F}$ -GE180 for imaging activated microglia (18kD translocator protein ligand, TSPO), and static 30-60 min recordings with  $^{18}\text{F}$ -FDG for energy metabolism and  $^{18}\text{F}$ -florbetaben for amyloidosis. Optimal fusion of PET data was obtained through automatic non-linear spatial normalization, and standardized-uptake-value-ratios (SUVR) were calculated. For the novel TSPO tracer  $^{18}\text{F}$ -GE180, we then calculated distribution volume ratios (DVR) after establishing a suitable reference region. Immunohistochemical analyses with TSPO antisera, methoxy-X04 staining for fibrillary  $\beta$ -amyloid, and *ex vivo* autoradiography served as terminal gold standard assessments.

### **Results:**

SUVR at 60-90 min p.i. gave robust quantitation of  $^{18}\text{F}$ -GE180, which correlated well with DVR calculated from the entire recording, and using a white matter reference region. Relative to age-matched WT,  $^{18}\text{F}$ -GE180 SUVR was slightly elevated in PS2APP mice at five months (+9%;  $p < 0.01$ ), and distinctly increased

at 16 months (+25%;  $p < 0.001$ ). Over this age range, there was high positive correlation between  $\mu$ PET findings of microglial activation with amyloid load ( $R = 0.85$ ;  $p < 0.001$ ), and likewise with metabolism ( $R = 0.61$ ;  $p < 0.005$ ). Immunohistochemical and autoradiographic findings confirmed the *in vivo*  $\mu$ PET data.

**Conclusion:**

In this first triple tracer  $\mu$ PET in a well-established AD mouse model, we find evidence for age-dependent microglia activation. This activation, correlating positively with the amyloid-load, implies a relationship between amyloidosis and inflammation in the PS2APP AD mouse model.

**Keywords:** neuroinflammation; TSPO; small animal PET;  $^{18}\text{F}$ -GE180;

Alzheimer's disease

## INTRODUCTION

Alzheimer's disease (AD) is the most common cause of dementia, with its exponentially increasing incidence as a function of age among the elderly, it is imposing an ever more onerous burden on health care (1). This state of affairs motivates a worldwide effort to find new biomarkers predicting future cognitive decline in patients with suspicious of early AD, and likewise for use as outcome measures in clinical trials of innovative disease-modifying agents (2). Immunologically-mediated neuroinflammation is implicated in the pathophysiological processes of AD (3, 4), which are classically characterized by accumulation of extracellular  $\beta$ -amyloid plaques and intracellular neurofibrillary tangles (5). Many aspects of the classical  $\beta$ -amyloid pathology are emulated in various transgenic rodent models for AD (6, 7); and translational studies of these processes are facilitated by small animal positron-emission-tomography ( $\mu$ PET) using radioligands for imaging of AD biomarkers in these rodent models (8). In particular,  $\mu$ PET imaging of  $\beta$ -amyloid has been successfully established in the past few years (9, 10). However, information regarding neuroinflammation in these models remains sparse and rather inconsistent (11-13).

Neuroinflammation can be assessed by molecular imaging with several  $^{11}\text{C}$  labelled radiotracers targeting the 18kD translocator protein (TSPO), which is highly expressed at the outer mitochondrial membrane of activated microglia (14, 15); the brief physical half-life of Carbon-11 presents logistic difficulties for its widespread use. However, novel  $^{18}\text{F}$ -fluorinated second-generation TSPO radiotracers now offer a more practical means to undertake imaging also at sites

lacking a cyclotron/radiochemistry facility. Among the various such compounds,  $^{18}\text{F}$ -GE180 has emerged as a TSPO ligand affording excellent signal-to-noise ratio and brain kinetics favourable for the detection of microglia activation (16, 17). However, monitoring of neuroinflammation in AD mice by this agent remains to be established.

The aim of this study was to investigate the novel TSPO tracer  $^{18}\text{F}$ -GE180 in PS2APP mice, a well-established transgenic AD mouse model; we have previously characterised by  $^{18}\text{F}$ -florbetaben  $\mu\text{PET}$  the progressive amyloid plaque formation with aging in this strain (18). We now carried out  $^{18}\text{F}$ -GE180  $\mu\text{PET}$  examinations in groups of transgenic (TG) and WT (WT) mice at various ages, and also measured  $\beta$ -amyloid using  $^{18}\text{F}$ -florbetaben and glucose metabolism  $^{18}\text{F}$ -FDG. With this multi-tracer approach we undertook to chart the interrelations of all three biomarkers *in vivo* during the life-course of PS2APP mice in order to test the hypothesis of a potential coherence between neuroinflammation and amyloidosis. In particular we anticipated that amyloidosis in TG PS2APP mice should result in greater inflammation, bringing in turn increased glucose metabolism. We confirmed the  $^{18}\text{F}$ -GE180  $\mu\text{PET}$  results relative to gold standard findings obtained by immunohistochemistry and additionally by autoradiography *ex vivo* in a subset of animals.

## **MATERIALS AND METHODS**

### **Radiochemistry**

*$^{18}\text{F}$ -GE180*: Radiosynthesis of  $^{18}\text{F}$ -GE180 was performed as previously described

(17), with slight modifications as presented in Supplementary Methods. This procedure yielded a radiochemical purity exceeding 98%, and a specific activity of  $1400 \pm 500$  GBq/ $\mu$ mol at end of synthesis.

*<sup>18</sup>F-Florbetaben and <sup>18</sup>F-FDG:* Radiosynthesis of <sup>18</sup>F-florbetaben was performed as previously described (10). This procedure yielded a radiochemical purity exceeding 98%, and a specific activity of  $80 \pm 20$  GBq/ $\mu$ mol at end of synthesis. <sup>18</sup>F-FDG was purchased commercially.

## **Animals**

All experiments were carried out in compliance with the National Guidelines for Animal Protection, Germany and the approval of the regional animal care committee (Regierung Oberbayern), and were overseen by a veterinarian. Animals were housed in a temperature- and humidity-controlled environment with a 12-h light–dark cycle, with free access to food (Ssniff, Soest, Germany) and water.

The transgenic B6.PS2APP (line B6.152H) is homozygous for the human presenilin (PS) 2, N141I mutation and also the human amyloid precursor protein (APP) K670N, M671L mutation. The APP and PS2 transgenes are driven by mouse Thy-1 and mouse prion promoters, respectively. This line had been created by co-injection of both transgenes into C57Bl/6 zygotes (19). Homozygous B6.PS2APP (PS2APP) mice show first appearance of plaques in the cortex and hippocampus at five to six months of age (20).

## **Study Overview**

The study design consisted of a pilot study and the main study.

In the pilot study, autoradiography *ex vivo* and *in vitro* was performed with <sup>18</sup>F-GE180, followed by immunohistochemistry in small groups of WT and TG mice at 10 and 22 months of age.

In the main study,  $\mu$ PET scans were obtained with the three radiopharmaceuticals described in groups of WT and TG mice aged 5, 8, 13, and 16 months ( $\pm 0.5$  months). Within one week after completion of the PET session, mice were perfused with phosphate buffered saline while deeply anesthetized prior to immunohistochemical analyses. A detailed overview for the main study of the different groups of mice is provided in Table 1. To investigate reproducibility of results with <sup>18</sup>F-GE180, we undertook test-retest PET scans in a subset of eleven TG animals (aged 5-16 months; N=2-3 at each time point) at an interval of one week to allow recovery from anaesthesia.

## **$\mu$ PET Data Acquisition, Reconstruction, and Co-registration**

Details of the acquisition protocol and reconstruction algorithms as well as co-registration procedures are provided in Supplementary Methods.

## **$\mu$ PET Data Analyses**

Volumes-of interest (VOIs) were defined on the MRI mouse atlas (Fig. 1). A large forebrain target VOI (comprising 156 mm<sup>3</sup>), containing most of the frontal and

parietal cortex as well as the hippocampus and the thalamus was used for all tracers. For reference region analysis in the case of  $^{18}\text{F}$ -GE180  $\mu\text{PET}$ , we tested several different tissue compartments. The reference regions consisted of a whole brain VOI (comprising  $525\text{ mm}^3$ ), and a whole cerebellar VOI (comprising  $65\text{ mm}^3$ ), as described previously(21). We also tested oval shaped white matter VOI mostly containing white matter tissue of the cerebellum and the brainstem (comprising  $29\text{ mm}^3$ ), which emerged by voxel-wise mapping of the contrast between WT and TG and WT groups, as described in detail in the Supplementary Methods and illustrated in Supplemental Fig. 1.

Based on our previous experience, the entire cerebellum was used for scaling of  $^{18}\text{F}$ -FDG data. For  $^{18}\text{F}$ -florbetaben a different white matter reference region ( $67\text{ mm}^3$ ; pons, midbrain, hindbrain parts of the subcortical white matter) emerged superior to scaling by the cerebellum in a not yet published in house investigation, such that we already switched the amyloid-PET analysis to this reference region. In animals receiving the full dynamic  $^{18}\text{F}$ -GE180  $\mu\text{PET}$  scan, distribution volume ratios (DVR) maps were calculated using a linear graphic method (22), relative to a white matter VOI intended to serve as a pathology-free reference tissue. We extracted and compared time activity-curves (TACs) of the several target and reference VOIs.

Standardized uptake values (SUV) for target and reference VOIs were calculated by scaling to the injected dose and multiplying the body weight for  $^{18}\text{F}$ -GE180. Forebrain target-to-reference tissue SUV ratios (SUVR) were employed for

calculation of  $SUVR_{FBR/REF}$  for the case of dynamic  $^{18}\text{F}$ -GE180 scans, and for the static frames for the cases of all of  $^{18}\text{F}$ -florbetaben and  $^{18}\text{F}$ -FDG.

### ***Ex Vivo and In Vitro* Autoradiography**

In the pilot study, autoradiography experiments were carried out to confirm the specificity of  $^{18}\text{F}$ -GE180  $\mu\text{PET}$  results to TSPO distribution. Autoradiography *ex vivo* was performed in two TG mice aged 22 months at 60 min after injection of 9.2 MBq  $^{18}\text{F}$ -GE180 (+150  $\mu\text{l}$  saline). *In vitro* autoradiography with  $^{18}\text{F}$ -GE180 at a range of concentrations (with and without blocking by TSPO antibody) and  $^{18}\text{F}$ -florbetaben was performed in brain cryostat sections from the pilot study subset of aged TG mice. Details of the autoradiography procedures are provided in Supplementary Methods.

### **Immunohistochemistry: Acquisition and Image Analysis**

Plaque and microglia load were calculated as the summed area of all labelled plaques and microglia, and reported as percentage densities relative to the entire cerebral cortex areas. These analyses were performed by an operator who was blind to the  $\mu\text{PET}$  results. Methodological details can be found in Supplementary Methods.

### **Statistics**

Group comparisons of VOI-based  $\mu\text{PET}$  results between WT and TG mouse groups were assessed by one-way analysis of variance (ANOVA) and Tukey

post-hoc test for multiple comparisons IBM SPSS Statistics (version 22.0; SPSS, Chicago, IL). For correlation analyses, Pearson's coefficients of correlation (R) were calculated. A threshold of  $p < 0.05$  was considered to be significant for rejection of the null hypothesis.

## **RESULTS**

### **Validation of $^{18}\text{F}$ -GE180 PET**

VOI based analyses were performed with the dynamic dataset in order to establish the kinetics of  $^{18}\text{F}$ -GE180 in target tissues of WT and TG animals, and to define optimal time-windows and reference tissue normalization for routine  $\mu\text{PET}$  examinations.

TACs for  $^{18}\text{F}$ -GE180 in several reference tissues, calculated as SUV (mean  $\pm$  SD) in TG mice at different ages are shown in Fig. 2A. Age dependence of the TACs is conspicuous with whole brain and whole cerebellar scaling, whereas the white matter reference tissue yielded a distinctly higher congruence between animal groups. Mean white matter reference SUV in the interval 60-90 min p.i. was similar in TG and WT of all ages (range of mean SUV: 2.98–3.16; range of SUV SD: 0.44–0.58; no significant inter-group differences).

No relevant spill-in of extracerebral activity to the brain was observed during the entire 90 min emission sequences. The reference tissue ratio TACs revealed an equilibrium binding in brain occurring by 20 minutes for the aged TG groups (13 and 16 months), whereas younger TG groups (5 and 8 months) indicated a slight but constant decline in cerebral activity, with a trend towards apparent equilibrium

in the last two frames. Thus, as an alternative to kinetic modelling for  $^{18}\text{F}$ -GE180 quantification, the use of SUVR in a static frame recorded in the interval 60-90 min p.i. provides a convenient surrogate maker for specific binding (Fig. 2B).

In this regard there was excellent linear relationship between DVR, calculated for the entire 90 minute recording, and the 60-90 min static frame SUVR ( $R=0.99$ ,  $p<0.001$ ) (Fig. 2C). Test-retest analyses confirmed as well the robustness of 60-90 min  $\text{SUVR}_{\text{FBR/WM}}$  for the forebrain target region in TG animals (best fit:  $R=0.98$ , linear,  $p<0.001$ ; test-retest variability 1.9%).

Variance in the forebrain  $^{18}\text{F}$ -GE180 SUVR for the 60-90 min static recording within groups of mice was distinctly lower in conjunction with a white matter reference region (mean SD:  $4.5\pm 1.0\%$ ; range: 3.0–5.9%), compared to the plain SUV (mean SD:  $15.7\pm 4.7\%$ ; range: 8.8–21.2%; Fig. 2D).

### **Triple Tracer $\mu\text{PET}$ analyses**

All  $\mu\text{PET}$  results are provided in Table 1. TG mice already showed elevated  $\text{SUVR}_{\text{FBR/WM}}$   $^{18}\text{F}$ -GE180 uptake when compared to age matched WT mice as early as five months (+9%;  $p<0.005$ ), which increased substantially by 16 months (+25%;  $p<0.001$ ) (Fig. 3).  $^{18}\text{F}$ -florbetaben  $\text{SUVR}_{\text{FBR/CBL}}$  in TG mice was near the WT level at five and eight months (+2%, +4%;  $p=\text{n.s.}$ ), and increased at 13 months (+15%;  $p<0.001$ ), and 16 months (+24%;  $p<0.001$ ) to age-matched WT mice.  $^{18}\text{F}$ -FDG  $\text{SUVR}_{\text{FBR/CBL}}$  was significantly higher in PS2APP TG mice at all ages when compared to age-matched WT groups, with the peak increase at eight

months (+12%;  $p < 0.001$ ), which subsequently declined in the 16 month group (+5%;  $p < 0.05$ ).

There was an excellent positive correlation ( $R = 0.85$ ;  $p < 0.001$ ) between  $^{18}\text{F}$ -GE180  $\text{SUVR}_{\text{FBR/WM}}$  and  $^{18}\text{F}$ -florbetaben  $\text{SUVR}_{\text{FBR/CBL}}$  in the pooled PS2APP TG mice. Lesser correlations were seen between  $^{18}\text{F}$ -FDG  $\text{SUVR}_{\text{FBR/CBL}}$  and  $^{18}\text{F}$ -GE180  $\text{SUVR}_{\text{FBR/WM}}$  and ( $R = 0.61$ ;  $p < 0.005$ ) and also  $^{18}\text{F}$ -florbetaben  $\text{SUVR}_{\text{FBR/CBL}}$  ( $R = 0.48$ ;  $p < 0.01$ ) (Fig. 4). WT indicated a high positive correlation between  $^{18}\text{F}$ -FDG  $\text{SUVR}_{\text{FBR/CBL}}$  and  $^{18}\text{F}$ -GE180  $\text{SUVR}_{\text{FBR/WM}}$  ( $R = 0.55$ ;  $p < 0.005$ ). No significant associations between  $^{18}\text{F}$ -FDG  $\text{SUVR}_{\text{FBR/CBL}}$  or  $^{18}\text{F}$ -GE180  $\text{SUVR}_{\text{FBR/WM}}$  with  $^{18}\text{F}$ -florbetaben  $\text{SUVR}_{\text{FBR/CBL}}$  were observed. The age dependence in the uptake of the three tracers is presented in Fig. 5.

### **Autoradiography and Immunohistochemistry**

IBA-1 antibody *in vitro* quantitation (occupancy(%)) in the whole group of PS2APP mice showed strong positive correlation with the  $^{18}\text{F}$ -GE180 uptake *in vivo* ( $R = 0.61$ ;  $p < 0.005$ ).  $^{18}\text{F}$ -florbetaben uptake and percentage plaque load (%) as assessed by methoxy-X04 histology had an very high correlation finding ( $R = 0.80$ ;  $p < 0.001$ ), as in our previous  $\beta$ -amyloid-PET studies (10, 18). Both immunohistochemical staining methods indicated a progression of pathophysiology with age in a manner congruent with the PET data (Supplemental Fig. 2).

The pattern of  $^{18}\text{F}$ -GE180 binding seen by autoradiography *ex vivo* resembled the binding observed in the  $\mu\text{PET}$  scan, and triple labelling *in vitro* showed co-

localization of TSPO activation with fibrillar  $\beta$ -amyloid deposits (Fig. 6). Qualitatively, the  $^{18}\text{F}$ -GE180 autoradiography *in vitro* was more diffuse than for  $^{18}\text{F}$ -florbetaben, which showed a more focal pattern. Prior incubation of brain sections with TSPO antibody completely blocked  $^{18}\text{F}$ -GE180 labelling in the forebrain, thus indicating the specific association of increased TSPO expression and amyloid plaques (Supplemental Fig. 3).

## **DISCUSSION**

We present the first small animal PET study with three different  $^{18}\text{F}$ -labelled radiotracers targeting distinct aspects of the pathophysiology in a transgenic mouse model of AD, i.e. microglial activation, amyloid deposition, and brain energy metabolism. The novel TSPO ligand  $^{18}\text{F}$ -GE180 enabled a robust detection of activated microglia in the TG mouse brain, yielding results concurring closely with immunohistochemical findings and autoradiography *in vitro*. The consensus of our results clearly indicates coexistence of amyloidosis and neuroinflammation in PS2APP TG mice, together increasing in parallel with increasing age. These findings are seemingly accompanied by elevated glucose consumption.

### **$^{18}\text{F}$ -GE180 reference region**

One key issue in detecting microglial activation by PET is the lack of an appropriate pathology-free reference tissue, i.e. a region devoid of TSPO expression in mouse brain (23). In the absence of a “true” reference region, a

recent PET study of TSPO expression in AD patients showed clear benefits for a SUVR analysis with the cerebellum as a pseudo-reference region, compared to quantitation relative to arterial blood input for  $^{11}\text{C}$ -PBR28 (24). Therefore, we tested several reference tissues for our novel ligand for TSPO,  $^{18}\text{F}$ -GE180. Our analyses revealed that a reference region composed of white matter voxels in brainstem and cerebellum delivered comparable SUV results between TG and WT groups at different ages. In contrast the whole brain and, to a lesser degree, the cerebellum showed elevated SUV in TG mice with marked pathology, thus being less suitable as a reference region. The white matter reference VOI was of a size ( $29\text{mm}^3$ ) sufficient to minimize signal loss due to partial volume effects (25). Furthermore, the SUVR approach distinctly minimized the intragroup variance in TSPO results compared to that with simple SUV calculation, which is in line with findings from the human study cited above (24). Thus we see a clear advantage for a cerebral pseudo-reference region in the semi-quantitative analysis of preclinical TSPO imaging.

### **$^{18}\text{F}$ -GE180 time window**

$^{18}\text{F}$ -GE180  $\mu\text{PET}$  showed uptake throughout the mouse brain, and only minor uptake in extracerebral regions such as cranium or Harderian glands relative to the brain. Ratio analysis of the measured TACs revealed attainment of stable values in aged TG animals as early as 20 minutes post injection, whereas ratio TACs in younger TG animals tended to have a more delayed stabilization in late acquisition frames after 50 minutes, favouring the use of late static window in

routine acquisitions. The DVR results using the entire 90 min recordings had an excellent correlation with the SUVR in the 60-90 min static frame, which further supports the use of this time window for economic  $\mu$ PET imaging in large study groups.

### **Neuroinflammation in the TG mouse model of AD**

Age-dependent increases in TSPO expression emerged as a clear surrogate for neuroinflammation in PS2APP mice, and clearly reveal a temporal association with the amyloid cascade. Our findings of 25% elevated  $SUVR_{WM}$  for  $^{18}F$ -GE180 in aged TG mice compared to WT mice indicates a satisfactory signal-to-noise ratio for  $^{18}F$ -GE180, while *in vivo* findings matched closely with TSPO immunohistochemistry *in vitro*. A very recent study with the same radiotracer in another AD mouse model (APP/PS1dE9) found similar age-dependent microglial activation in cortex and hippocampus matching with terminal immunohistochemistry findings (26). Present findings are also in line with a recent report of elevated neuroinflammation in brain of aged APPswePS1-dE9 mice as examined by  $^{18}F$ -DPA-714  $\mu$ PET (13) as was also confirmed in autoradiographic and immunohistochemical analyses. Our results show a close correlation between accumulation of amyloid load and TSPO expression in PS2APP mice, where the causal relationship is still under debate (27) and we speculate about this issue in the Supplemental Discussion. Remarkably, our PS2APP mice do not indicate a relevant neurodegeneration at 16 months of age (19), even though they show severe neuroinflammation and amyloid pathology.

Furthermore normalized  $^{18}\text{F}$ -FDG uptake,  $\mu\text{PET}$  marker for glucose metabolism, was elevated in PS2APP mice especially in the young group, and to a lesser extent still at 16 months of age, compared to findings in WT groups. This seems in line with previous reports of elevated relative glucose metabolism in amyloid models, like APP/PS1 (28) and 5xFAD (29) mice, where glial activation was discussed as a probable factor. However, this interpretation seems at odds with  $^{18}\text{F}$ -FDG findings in human AD, and in prodromal patients with amnesic mild cognitive impairment (30). Nonetheless there is even evidence about metabolic compensation in AD (31), where the synaptic dysfunction might mask inflammatory related hypermetabolism.

### ***In vivo* therapy monitoring**

In our hands, microglial activation and amyloid levels as assessed by  $\mu\text{PET}$  had high inter-animal variability as has been reported for other AD mouse models (32). Therefore the sensitivity of terminal assessments of treatment effects on neuroinflammation or amyloidogenesis would likely be hampered by this variance. This circumstance emphasizes the value of a reliable non-invasive treatment monitoring, which offers the possibility to account for baseline pathology levels at therapy initiation, and also allows the detection of longitudinal changes in individual mice, as shown in our recent anti-amyloid treatment  $\mu\text{PET}$  study (33). Neuroinflammation constitutes an interesting therapy target in its own right and present results with  $^{18}\text{F}$ -GE180  $\mu\text{PET}$  show considerable promise for this application.

## **Limitations**

This was a cross-sectional study in groups of mice from the same breeding program; a true longitudinal setting would have entailed serial  $\mu$ PET examinations for each biomarker in each mouse. This would have required twelve  $\mu$ PET scans per mouse, likely resulting in an increased incidence of dropouts, and without the possibility of performing immunohistochemical validation in each mouse for all ages. Additionally, we feel that this limitation is balanced by the adequately-powered sample sizes, which yielded results sufficiently robust to detect significant differences even between mouse groups at five months of age.

## **CONCLUSION**

*In vivo* imaging of neuroinflammation by  $\mu$ PET with the novel TSPO ligand  $^{18}\text{F}$ -GE180 is feasible, and results correlate strongly with immunohistochemical gold standard assessment, with further support by autoradiographic findings *ex vivo*. Single frame recordings at 60-90 min p.i. yield robust and reproducible SUVR values that shall bring considerable economy to  $\mu$ PET studies with large group size. In PS2APP mice age-dependent amyloid accumulation, revealed by  $^{18}\text{F}$ -florbetaben, occurs in conjunction with inflammation, assessed by  $^{18}\text{F}$ -GE180  $\mu$ PET, respectively. Glucose metabolism as assessed by  $^{18}\text{F}$ -FDG  $\mu$ PET correlated positively with inflammation, but hypermetabolism relative to WT mice

was pronounced in young TG mice. This illustrates a concomitant inflammatory process in association with the amyloidosis in this transgenic AD mouse model.

## **ACKNOWLEDGMENTS**

A part of this paper originated from the doctoral thesis of Federico Probst. We thank Karin Bormann-Giglmaier and Rosel Oos for excellent technical assistance. Florbetaben precursor was provided by Piramal Imaging. GE180 cassettes were received from GE. We acknowledge textual revisions by Inglewood Biomedical Editing.

## References

1. Ziegler-Graham K, Brookmeyer R, Johnson E, Arrighi HM. Worldwide variation in the doubling time of Alzheimer's disease incidence rates. *Alzheimers Dement.* 2008;4:316-323.
2. Weiner MW, Veitch DP, Aisen PS, et al. The Alzheimer's Disease Neuroimaging Initiative: A review of papers published since its inception. *Alzheimers Dement.* 2012;8:S1-S68.
3. Heneka MT, Carson MJ, El Khoury J, et al. Neuroinflammation in Alzheimer's disease. *Lancet Neurol.* 2015;14:388-405.
4. McGeer PL, McGeer EG. Mechanisms of cell death in Alzheimer disease--immunopathology. *J Neural Transm Suppl.* 1998;54:159-166.
5. Duyckaerts C, Delatour B, Potier MC. Classification and basic pathology of Alzheimer disease. *Acta Neuropathol.* 2009;118:5-36.
6. Hall AM, Roberson ED. Mouse models of Alzheimer's disease. *Brain Res Bull.* 2012;88:3-12.

7. Teipel SJ, Buchert R, Thome J, Hampel H, Pahnke J. Development of Alzheimer-disease neuroimaging-biomarkers using mouse models with amyloid-precursor protein-transgene expression. *Prog Neurobiol.* 2011;95:547-556.
8. Zimmer ER, Parent MJ, Cuello AC, Gauthier S, Rosa-Neto P. MicroPET imaging and transgenic models: a blueprint for Alzheimer's disease clinical research. *Trends Neurosci.* 2014;37:629-641.
9. Manook A, Yousefi BH, Willuweit A, et al. Small-animal PET imaging of amyloid-beta plaques with [11C]PiB and its multi-modal validation in an APP/PS1 mouse model of Alzheimer's disease. *PLoS One.* 2012;7:e31310.
10. Rominger A, Brendel M, Burgold S, et al. Longitudinal assessment of cerebral beta-amyloid deposition in mice overexpressing Swedish mutant beta-amyloid precursor protein using 18F-florbetaben PET. *J Nucl Med.* 2013;54:1127-1134.
11. Rapic S, Backes H, Viel T, et al. Imaging microglial activation and glucose consumption in a mouse model of Alzheimer's disease. *Neurobiol Aging.* 2013;34:351-354.
12. Rodriguez-Vieitez E, Ni R, Gulyas B, et al. Astrocytosis precedes amyloid plaque deposition in Alzheimer APP<sup>swe</sup> transgenic mouse brain: a correlative

positron emission tomography and in vitro imaging study. *Eur J Nucl Med Mol Imaging*. 2015.

**13.** Serriere S, Tauber C, Vercouillie J, et al. Amyloid load and translocator protein 18 kDa in APP<sup>swe</sup>PS1-dE9 mice: a longitudinal study. *Neurobiol Aging*. 2015;36:1639-1652.

**14.** Cumming P, Pedersen MD, Minuzzi L, et al. Distribution of PK11195 binding sites in porcine brain studied by autoradiography in vitro and by positron emission tomography. *Synapse*. 2006;59:418-426.

**15.** Zimmer ER, Parent MJ, Cuellar AC, Gauthier S, Rosa-Neto P. MicroPET imaging and transgenic models: a blueprint for Alzheimer's disease clinical research. *Trends Neurosci*. 2014.

**16.** Dickens AM, Vainio S, Marjamaki P, et al. Detection of microglial activation in an acute model of neuroinflammation using PET and radiotracers <sup>11</sup>C-(R)-PK11195 and <sup>18</sup>F-GE-180. *J Nucl Med*. 2014;55:466-472.

**17.** Wickstrom T, Clarke A, Gausemel I, et al. The development of an automated and GMP compliant FASTlab Synthesis of [(18) F]GE-180; a radiotracer for imaging translocator protein (TSPO). *J Labelled Comp Radiopharm*. 2014;57:42-48.

- 18.** Brendel M, Jaworska A, Griessinger E, et al. Cross-sectional comparison of small animal [18F]-florbetaben amyloid-PET between transgenic AD mouse models. *PLoS One*. 2015;10:e0116678.
- 19.** Richards JG, Higgins GA, Ouagazzal AM, et al. PS2APP transgenic mice, coexpressing hPS2mut and hAPPswe, show age-related cognitive deficits associated with discrete brain amyloid deposition and inflammation. *J Neurosci*. 2003;23:8989-9003.
- 20.** Ozmen L, Albientz A, Czech C, Jacobsen H. Expression of transgenic APP mRNA is the key determinant for beta-amyloid deposition in PS2APP transgenic mice. *Neurodegener Dis*. 2009;6:29-36.
- 21.** Brendel M, Delker A, Rotzer C, et al. Impact of partial volume effect correction on cerebral beta-amyloid imaging in APP-Swe mice using [(18)F]-florbetaben PET. *Neuroimage*. 2014;84:843-853.
- 22.** Logan J, Fowler JS, Volkow ND, Wang GJ, Ding YS, Alexoff DL. Distribution volume ratios without blood sampling from graphical analysis of PET data. *J Cereb Blood Flow Metab*. 1996;16:834-840.

- 23.** Pedersen MD, Minuzzi L, Wirenfeldt M, et al. Up-regulation of PK11195 binding in areas of axonal degeneration coincides with early microglial activation in mouse brain. *Eur J Neurosci.* 2006;24:991-1000.
- 24.** Lyoo CH, Ikawa M, Liow JS, et al. Cerebellum Can Serve As a Pseudo-Reference Region in Alzheimer Disease to Detect Neuroinflammation Measured with PET Radioligand Binding to Translocator Protein. *J Nucl Med.* 2015;56:701-706.
- 25.** Constantinescu CC, Mukherjee J. Performance evaluation of an Inveon PET preclinical scanner. *Phys Med Biol.* 2009;54:2885-2899.
- 26.** Liu B, Le KX, Park MA, et al. In Vivo Detection of Age- and Disease-Related Increases in Neuroinflammation by <sup>18</sup>F-GE180 TSPO MicroPET Imaging in Wild-Type and Alzheimer's Transgenic Mice. *J Neurosci.* 2015;35:15716-15730.
- 27.** Heneka MT, Carson MJ, Khoury JE, et al. Neuroinflammation in Alzheimer's disease. *Lancet Neurol.* 2015;14:388-405.
- 28.** Poisnel G, Herard AS, El Tannir El Tayara N, et al. Increased regional cerebral glucose uptake in an APP/PS1 model of Alzheimer's disease. *Neurobiol Aging.* 2012;33:1995-2005.

- 29.** Rojas S, Herance JR, Gispert JD, et al. In vivo evaluation of amyloid deposition and brain glucose metabolism of 5XFAD mice using positron emission tomography. *Neurobiol Aging*. 2013;34:1790-1798.
- 30.** Ewers M, Brendel M, Rizk-Jackson A, et al. Reduced FDG-PET brain metabolism and executive function predict clinical progression in elderly healthy subjects. *Neuroimage Clin*. 2014;4:45-52.
- 31.** Caroli A, Lorenzi M, Geroldi C, et al. Metabolic compensation and depression in Alzheimer's disease. *Dement Geriatr Cogn Disord*. 2010;29:37-45.
- 32.** Teipel SJ, Buchert R, Thome J, Hampel H, Pahnke J. Development of Alzheimer-disease neuroimaging-biomarkers using mouse models with amyloid-precursor protein-transgene expression. *Prog Neurobiol*. 2011.
- 33.** Brendel M, Jaworska A, Herms J, et al. Amyloid-PET predicts inhibition of de novo plaque formation upon chronic gamma-secretase modulator treatment. *Mol Psychiatry*. 2015;20:1179-1187.

## Figure Legends

Figure 1:

Definitions of forebrain (yellow), whole brain (orange), cerebellar (red), and white matter (purple) volumes-of-interest projected on the mouse brain MRI atlas in coronal and sagittal slices.

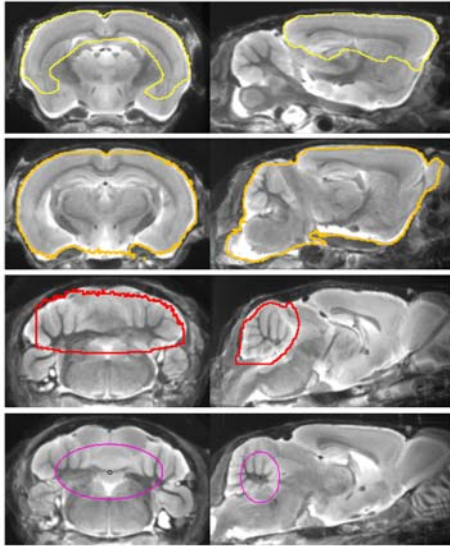


Figure 2:

(A) Mean  $^{18}\text{F}$ -GE180 uptake reported as SUV for each of three reference regions as functions of time following tracer administration in groups of PS2APP mice. The least evidence of pathology (i.e. stability between TG and WT) was detected for a white matter pseudo reference region. Error bars indicate SD for estimates in groups of 5-8 animals. (B) Target/reference ratios as functions of time following  $^{18}\text{F}$ -GE180 administration in groups of PS2APP mice. (C) Correlation of  $^{18}\text{F}$ -GE180 DVR calculated from 90 minute dynamic  $\mu\text{PET}$  recordings with corresponding SUVR (forebrain/white-matter) results from the 60-90 minute static frame. Dotted line represents a perfect line of identity (DVR = SUVR). (D) Stability of forebrain  $^{18}\text{F}$ -GE180 values after SUV calculation (blue) and pseudo reference tissue (orange) scaling as expressed by mean %-SD ( $\pm\text{SD}$ ) in all eight groups of TG and WT mice.

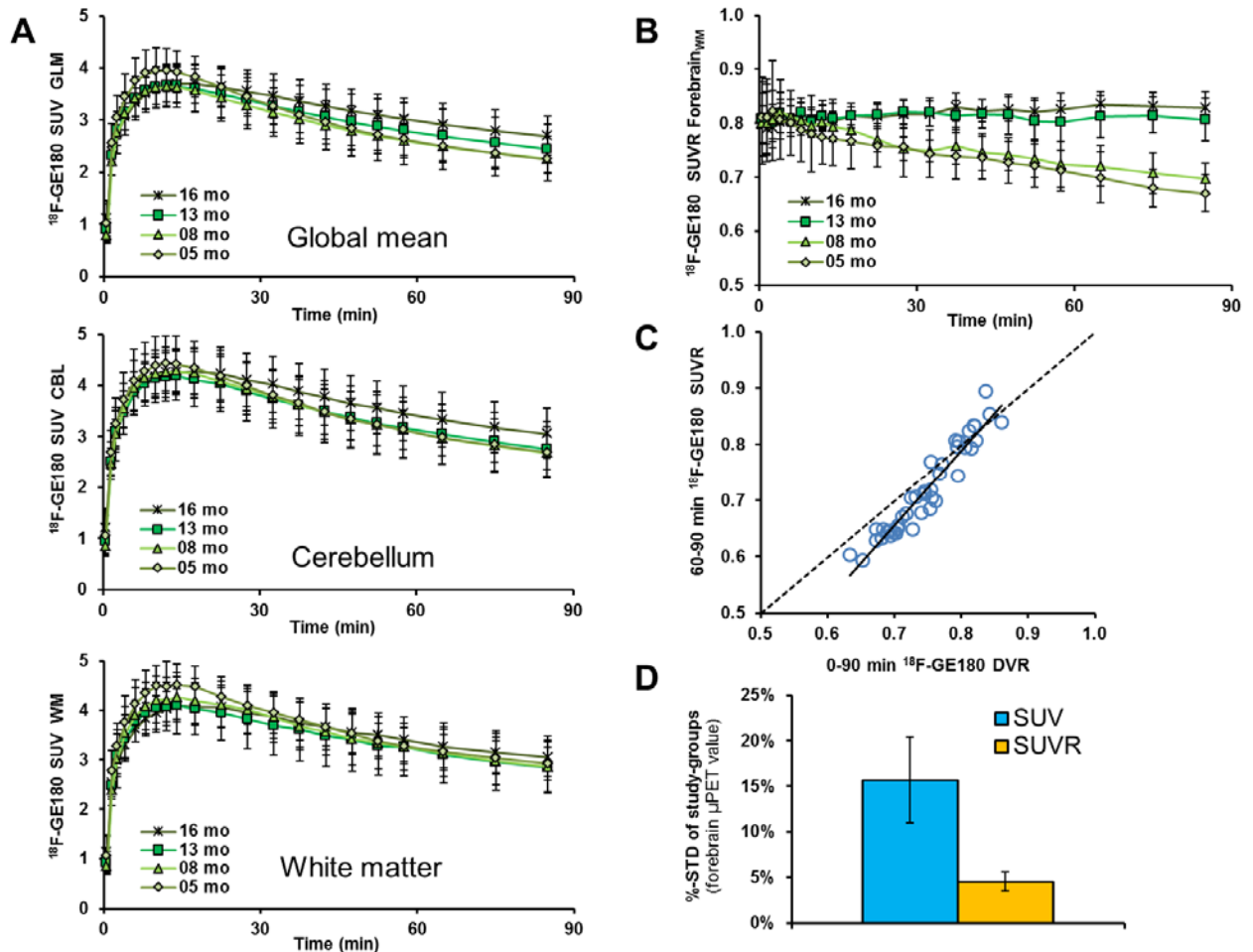


Figure 3:

(A) Coronal planes of  $^{18}\text{F}$ -GE180 mean SUVR maps at different ages of PS2APP animals projected upon an MRI mouse atlas (gray scale). (B) Mean ( $\pm$ SD) SUVR estimates for PS2APP animals at different ages. Significant differences between subgroups are marked by \*\*\*= $p < 0.001$ ; one-way ANOVA.

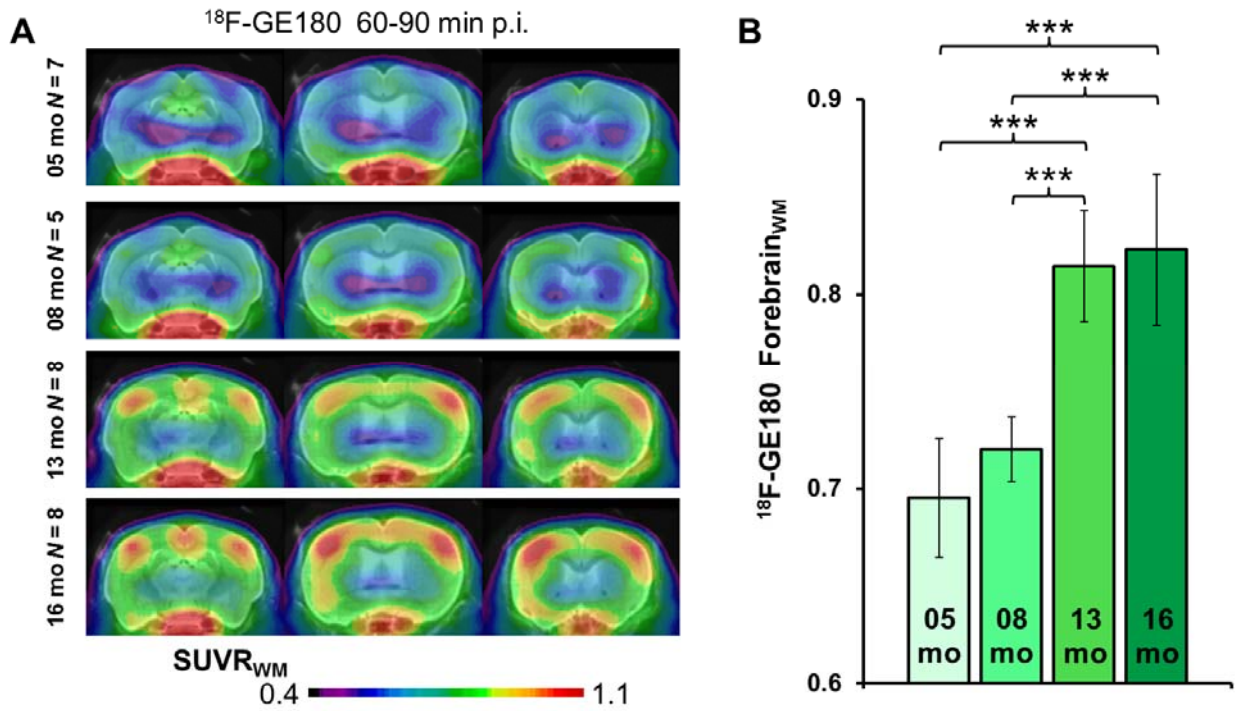
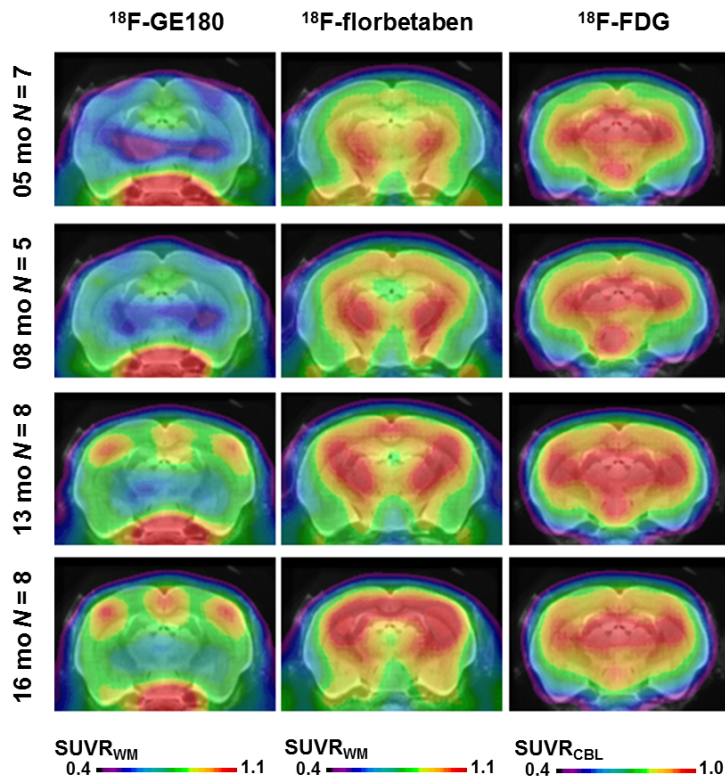


Figure 4:

(A) Coronal planes of mean SUVR maps for all three different radiotracers at different ages of PS2APP animals, projected upon an MRI mouse atlas (gray scale). (B) Correlations between the different forebrain radiotracer SUVR for all PS2APP mice.

**A**



**B**

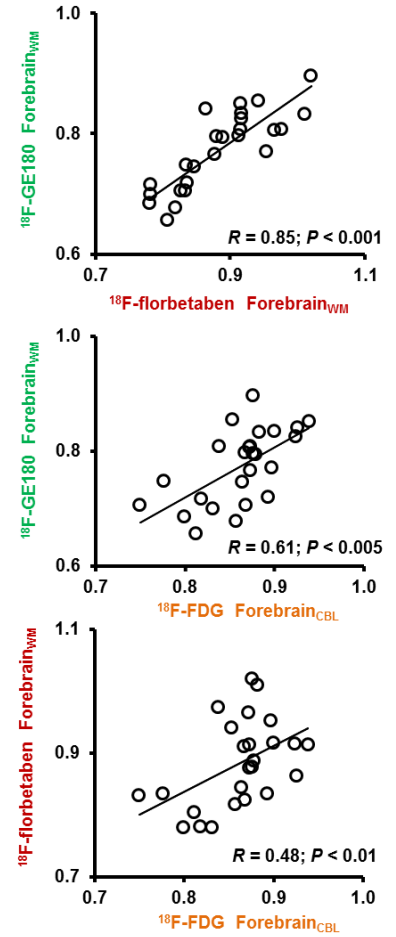


Figure 5:

Life-course kinetics for PS2APP mice as expressed by %-difference ( $\pm$ SD) versus C57Bl/6 controls for the three different radiotracers.

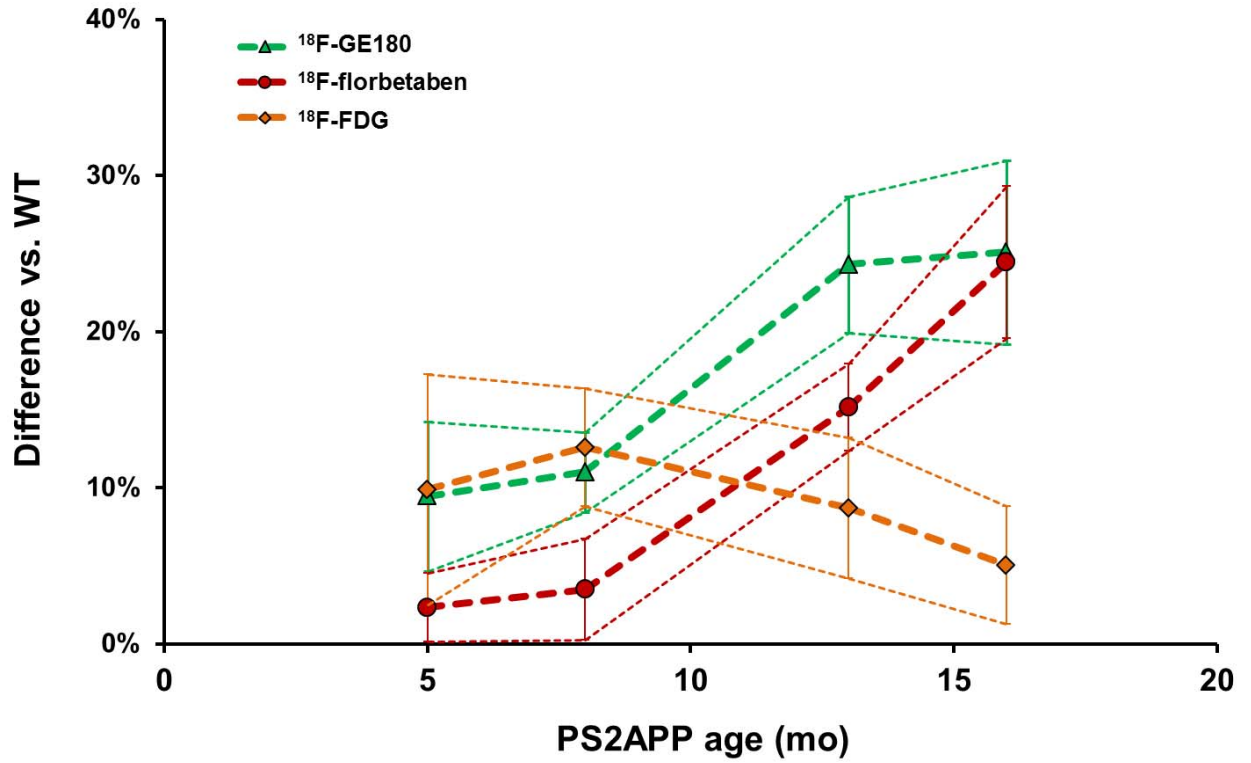


Figure 6:

(A) Immunohistochemical co-staining shows IBA-1 (red) and TSPO (green) positive cells adjacent (white circle) to fibrillar amyloid plaques (blue) in the frontal cortex of a PS2APP mouse aged 22 months. Yellow circle indicates low IBA-1 and TSPO staining between amyloid plaques. Scale bar represents 20 $\mu$ m.

(B) Sagittal plane for  $^{18}$ F-GE180 autoradiography *ex vivo* (60 min p.i.) in a 22 month old PS2APP mouse indicates extensive radiotracer uptake in the neocortex (red arrows), hippocampus and thalamus which is co-localized with (C) fibrillar amyloid as detected in the corresponding methoxy-X04 staining in these brain regions. No specific binding is observed in the cerebellum.

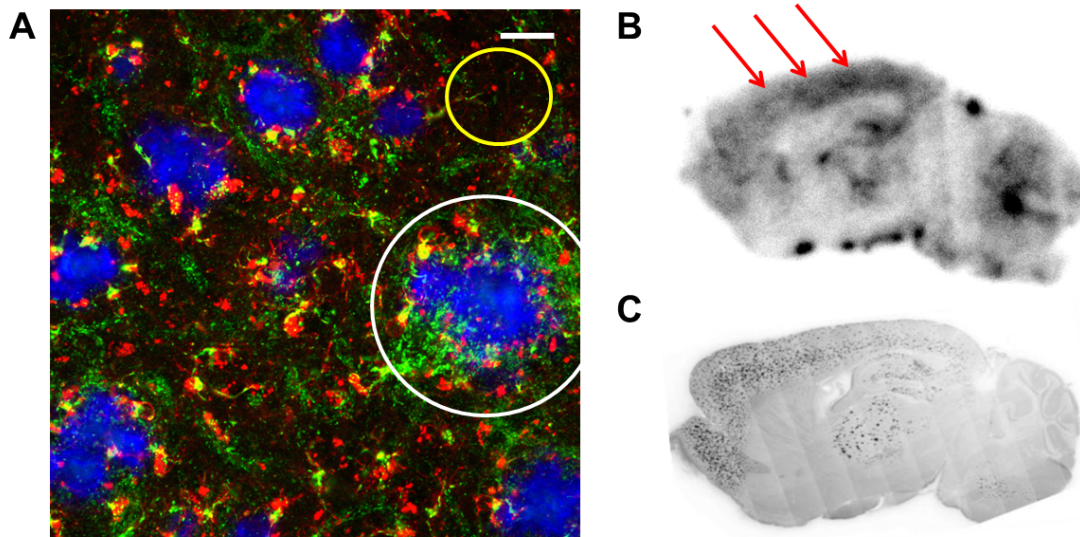


Table 1

Mouse Model	Age (mo)	<sup>18</sup> F-GE180 $\mu$ PET (N)	<sup>18</sup> F-GE180 $\mu$ PET (SUVR <sub>FBR/WM</sub> )	<sup>18</sup> F-florbetaben $\mu$ PET (N)	<sup>18</sup> F-florbetaben $\mu$ PET (SUVR <sub>FBR/WM</sub> )	<sup>18</sup> F-FDG $\mu$ PET (N)	<sup>18</sup> F-FDG $\mu$ PET (SUVR <sub>FBR/CBL</sub> )
PS2APP	5	6	0.69±0.03**	6	0.80±0.02	6	0.85±0.05***
	8	5	0.72±0.02***	4	0.82±0.03	4	0.90±0.05***
	13	8	0.81±0.03***	8	0.90±0.02***	8	0.94±0.02***
	16	8	0.83±0.04***	7	0.96±0.03***	7	0.91±0.03*
C57Bl/6	5	8	0.63±0.01	8	0.79±0.01	8	0.77±0.03
	8	8	0.65±0.03	8	0.79±0.01	8	0.80±0.03
	13	8	0.66±0.02	8	0.78±0.02	8	0.86±0.04***
	16	8	0.67±0.02*	8	0.78±0.02	8	0.86±0.04***

Study overview for the main study: Groups of PS2APP and C57Bl/6 mice are provided together with forebrain  $\mu$ PET SUVR values for the three radiotracers. Significant differences in PS2APP mice versus age-matched C57Bl/6 control or significant differences in C57Bl/6 controls against their five month old littermates are marked by \*=p<0.05; \*\*=p<0.01; \*\*\*=p<0.001; one-way ANOVA.